Fluid Dynamics & Materials Processing FDMP, vol.15, no.3, pp.207-231, 2019

Heat Absorption and Joule Heating Effects on Transient Free Convective Reactive Micropolar Fluid Flow Past a Vertical Porous Plate

MD. Shamshuddin[1, *] and C. Balarama Krishna[2]

Abstract: Mathematical model for an unsteady, incompressible, electrically conducting micropolar fluid past a vertical plate through porous medium with constant plate velocity has been investigated in the present study. Heat absorption, Joulian dissipation, and first-order chemical reaction is also considered. Under the assumption of low Reynolds number, the governing transport equations are rendered into non-dimensional form and the transformed first order differential equations are solved by employing an efficient finite element method. Influence of various flow parameters on linear velocity, microrotation velocity, temperature, and concentration are presented graphically. The effects of heat absorption and chemical reaction rate decelerate the flow is particularly near the wall. Skin friction and wall couple stress increases as heat absorption increases but the reverse phenomenon is observed in the case of chemical reaction rate. Wall mass transfer rate increases for chemical reaction and Sherwood number increases for heat absorption. Finite element study is very versatile in simulating unsteady micropolar rheo-materials processing transport phenomena. However, a relatively simple reaction effects restricted to first order.

Keywords: Heat absorption, joule heating, chemical reaction, micropolar fluid, finite element method.

Nomenclature

B_0	applied magnetic field strength $\left[A/m\right]$
C	concentration of the solute (mol m^{-3})
C_f	skin friction coefficient (Pa)
C_m	wall couple stress
C_p	specific heat at constant pressure (J kg^{-1} K^{-1})
C_w	concentration of the solute at the plate (mol m^{-3})
C_∞	concentration of the solute far away from the plate (Kg)
D_m	molecular diffusivity (m^2 K/W)

[1] Department of Mathematics, Vaagdevi College of Engineering (Autonomous), Warangal, Telangana, India.

[2] Department of Mathematics, S R Engineering College (Autonomous), Warangal, Telangana, India.

[*] Corresponding Author: MD. Shamshuddin. Email: shammaths@gmail.com.

Ec Eckert number
g^* acceleration due to gravity (m)
Gm species Grashof number
Gr thermal Grashof number
J dimensionless micro inertia coefficient
K permeability of the porous medium
Kr chemical reaction parameter
M magnetic field parameter
n non-dimensional oscillation frequency
Nu Nusselt number
p constant pressure
Pr Prandtl number
Q heat absorption parameter
q_r radiative heat flux
R radiation-conduction parameter
Re_x local Reynolds number
Sc Schmidt number
Sh_x Sherwood number
t non-dimensional time
T temperature of the field in the boundary layer
T_w wall temperature of the fluid
T_∞ temperature of the fluid far away from the plate
u^* velocity component along x-direction (m s^{-1})
u non-dimensional velocity component along x-direction
U_p dimensionless free stream velocity
U_∞ dimensionless free stream velocity
v^* velocity component along y-direction (m s^{-1})
v non-dimensional velocity component along the y-direction
V_o the scale of suction velocity
x^* axis along the plate (m)
y^* axis along the plate (m)

Greek Letters

β Eringen coupling number
β_f coefficient of thermal expansion (K^{-1})
β_c coefficient of concentration expansion (K^{-1})
ρ density of the magneto-micropolar fluid
σ electrical conductivity of the fluid

$\overline{\sigma}$ Stefen-Boltzmann constant
κ thermal conductivity of the medium
$\overline{k}$ mean absorption coefficient
ν kinematic viscosity
ν_r kinematic vortex viscosity
γ gyroscopic viscosity
Λ coefficient of gyro-viscosity
μ fluid dynamic viscosity
θ dimensionless temperature
ϕ dimensionless concentration
ψ shape function
ω microrotation component

1 Introduction

The flows in which electrically conducting gases or liquids interact with an applied magnetic field, in such flows Magnetohydrodynamics (MHD) are exploited. MHD features in a wide spectrum of modern industrial processes which includes nuclear heat transfer control, vortex control, power generators, etc. In recent years, natural convection flows with radiative, heat absorbing, and chemically reactive heat transfer have mobilized some interest, along with viscous dissipation and ohmic (Joule) heating has also prominent these days, in applications of materials fabrication operations. Damesh et al. [Damesh, Odat, Chamkha et al. (2009)] estimated an analysis to obtain an approximate solution using Runge-Kutta method to micropolar fluid flow over uniform stretched sheet considering heat generation/absorption and chemical reaction. Effects of magnetic field and heat absorption on a micropolar fluid by adopting the element-free Galerkin method was studied by Sharma et al. [Sharma, Bhargava and Singh (2010)] and Babu et al. [Babu, Lavanya and Ramanaiah (2015)], they presented various effects on a micropolar fluid considering stretching sheet. Rout et al. [Rout, Sahoo, Dash et al. (2016)] examined the effect of chemical reaction on free convection flow in a micropolar fluid. Pal et al. [Pal and Talukdar (2012)] studied analytically mixed convection periodic flow of a micropolar fluid considering chemical reaction and thermal radiation effects. Siva Reddy et al. [Siva Reddy and Shamshuddin (2015)] obtained a finite element solution for unsteady micropolar fluid flow in a rotating porous plate. Modather et al. [Modather, Rashad and Chamkha (2009)] examined the oscillatory flow of micropolar fluid on a vertical porous plate. Pal et al. [Pal and Biswas (2016)] extended the same flow considering thermal radiation and viscous dissipation effects, Roja et al. [Roja, Reddy and Reddy (2013)] study persuaded us to undertake present study. Several studies have examined study and unsteady flows with Joule and viscous dissipation effects can be seen in Babu et al. [Babu, Kumar and Reddy (2013); Chen (2004); Gebhert (1962); Rahman (2009); Ziaul Hoque, Mahmud Alam, Ferdows et al. (2012)]. Krishna et al. [Krishna and Rao (2014)] analyzed stability analysis for boundary value problems in differential equations, Further, Bala Rama Krishna et al. [Bala Rama Krishna, Rama Chandra Rao and Srikanth (2014)] used special multi-step method for solving non-linear boundary

value problems. Other recent applications of aforesaid studies considered in micropolar and nanofluid are Alam et al. [Alam, Islam and Uddin (2016); Singh and Kumar (2016); Rahman and Sultana (2016); Siva Reddy and Shamshuddin (2016); Siva Reddy and Thirupathi (2016a, 2016b, 2016c); Thirupathi, Anwar Beg and Kadir (2017a); Thirupathi, Chamkha and Siva Reddy (2017b); Thirupathi and Mishra (2018); Shamshuddin and Thirupathi (2017)].

Boundary value problems of various non-Newtonian fluid models have been solved numerically and analytically, which has been proposed to characterize the real fluid behavior. One such fluid is micropolar fluid, which exhibits microstructural characteristics like rotatory motions, gyration of fluid microelements. These fluids can support couple stresses, shear stresses, body couples and, also exhibit micro rotational effects and inertia due fluid bear dilute suspension of rigid macromolecules with individual motions. In the current trend among non-Newtonian fluids, Micropolar fluid has acquired special attention in numerous applications. Best-proven theories of fluids with microstructure was first brought in and formulated by Eringen [Eringen (1966)] and Cowin [Cowin (1968)] which has been applied in various fields in recent years. Later by generalizing micropolar fluids to heat conduction and other thermal effects, Eringen [Eringen (1966)] extended his theory and developed a new unified theory of mechanical materials. The hydrodynamic flow of micropolar fluids and their aspects are documented in Stokes [Stokes (1984)] and Lukaszewicz [Lukaszewicz (1999)]. More comprehensive detail of this theory and its applications can be found in Ariman et al. [Ariman, Turk and Sylvester (1973, 1974)].

To the best of our knowledge, above mentioned studies combined effect of heat absorption, chemical reaction and Joule heating on micropolar flows have not been much explored, this article presents these flows to obtain an approximate solution via widely accepted and robust Galerkin finite element technique to the perturbation approximate form solution presented by Roja et al. [Roja, Reddy and Reddy (2013)]. The mathematical formulation, method of solution and validation are presented in Sections 2, 3 and 4 respectively. Results and discussions are explored scientifically and experimentally in Section 5. Important results are summarized in the conclusion section. Finally, figures and tables are shown after the references section.

2 Mathematical formulation

The free convective flow of an incompressible electrically conducting micropolar fluid past a vertical porous plate is considered. The plate considered is permeable and is moving with constant velocity Up .Physical configuration is illustrated in Fig. 1. Initially, the temperature T_w and concentration C_w thereafter maintained as constant temperature T_∞^* and constant concentration C_∞^* . Darcy's law and low Reynolds number flow are assumed. Uniform magnetic field of strength B_0 is applied which is transverse to the flow direction. Though the Magnetic Reynolds number is very small, in comparison to the applied magnetic field the induced magnetic field is negligible [Cowling (1957)]. In comparison to the direction of y^* , the term radiative heat flux considered in x^*

direction is negligible. Since the plate is of infinite extent and electrically non-conducting all physical quantities, except pressure, depend on y^* and t^* only.

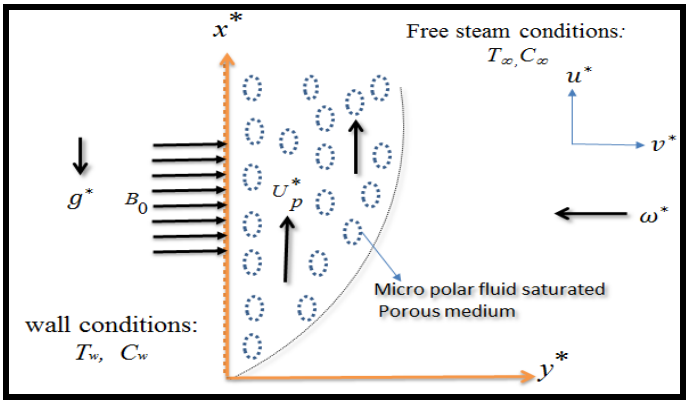

Figure 1: Flow configuration and coordinate system

By taking the aforesaid assumptions into consideration the governing boundary layer equations (see Roja et al. [Roja, Reddy and Reddy (2013)]) for unsteady convective micropolar fluid flow under Boussinesq's approximation are as follows:

$$\frac{\partial v^*}{\partial y^*} = 0 \tag{1}$$

$$\frac{\partial u^*}{\partial t^*} + v^* \frac{\partial u^*}{\partial y^*} = \left(\nu + \nu_r\right)\frac{\partial^2 u^*}{\partial y^{*2}} + g^*\beta_T\left(T^* - T_\infty\right) + g^*\beta_C\left(C^* - C_\infty\right) - \frac{\nu}{K^*}u^* - \frac{\sigma B_0^2 u^*}{\rho} + 2\nu_r\frac{\partial \omega^*}{\partial y^*} \tag{2}$$

$$\frac{\partial \omega^*}{\partial t^*} + v^* \frac{\partial \omega^*}{\partial y^*} = \frac{\gamma}{\rho\, j^*}\frac{\partial^2 \omega^*}{\partial y^{*2}} \tag{3}$$

$$\frac{\partial T^*}{\partial t^*} + v^* \frac{\partial T^*}{\partial y^*} = \frac{\kappa}{\rho C_p}\frac{\partial^2 T^*}{\partial y^{*2}} - \frac{1}{\rho C_p}\frac{\partial q_r}{\partial y^*} - \frac{Q^*}{\rho C_p}\left(T^* - T_\infty^*\right) + \frac{\nu + \nu_r}{C_p}\left(\frac{\partial u^*}{\partial y^*}\right)^2 + \frac{\sigma B_0^2}{\rho C_p}u^{*2} \tag{4}$$

$$\frac{\partial C^*}{\partial t^*} + v^* \frac{\partial C^*}{\partial y^*} = D_m\frac{\partial^2 C^*}{\partial y^{*2}} - K_r^*\left(C^* - C_\infty\right) \tag{5}$$

The following dimensional initial and boundary conditions are:

$$t^* \le 0 \quad \left\{ u^* = 0,\ \omega^* = 0,\ T^* = T_\infty^*,\ C^* = C_\infty^* \qquad for\ all\ y^* \ge 0 \right\}$$
$$t^* > 0 \quad \left\{ \begin{array}{ll} u^* = U_p^*\ , \omega^* = -\dfrac{\partial u^*}{\partial y^*},\ T^* = T_w^*,\ C^* = C_w^* & at\ \ y^* = 0 \\ u^* = U_\infty^*,\ \ \omega^* \to 0,\ \ T^* \to T_\infty^*,\ \ C^* \to C_\infty^* & as\ \ y^* \to \infty \end{array} \right\} \tag{6}$$

The following form is taken from Roja et al. [Roja, Reddy and Reddy (2013)]

$$v^* = -V_0 \tag{7}$$

where V_0 is suction velocity ($V_0 > 0$). The radiative heat flux term is described as follows

$$q_r = -\frac{4\bar{\sigma}}{3\bar{k}}\frac{\partial T^{*4}}{\partial y^*} \tag{8}$$

It is difficult to obtain the solution since Eq. (8) is highly nonlinear. Earlier several authors have obtained this problem assuming small temperature differences within the fluid flow [Adunson and Gebhert (1972); Raptis and Perdikis (1998)]. Using Taylor's series expansion about T^* neglecting higher order terms takes the form

$$T^{*4} \cong 4T_\infty^{*3} T^* - 3T_\infty^{*4} \tag{9}$$

Differentiating Eq. (8) w.r.t y^* and substituting in (10), we get

$$\frac{\partial q_r}{\partial y^*} = -\frac{16T_\infty^3\bar{\sigma}}{3\bar{k}}\frac{\partial^2 T}{\partial y^{*2}} \tag{10}$$

Now we introduced the following dimensionless variables and parameters:

$$\begin{array}{l} u = \dfrac{u^*}{U_0}, v = \dfrac{v^*}{V_0}, \eta = \dfrac{V_0 y^*}{\nu}, U_p = \dfrac{u_p^*}{U_0}, \omega = \dfrac{\nu}{U_0 V_0}\omega^*, t = \dfrac{t^* V_0^2}{\nu}, \theta = \dfrac{T^* - T_\infty^*}{T_w^* - T_\infty^*}, \\ \phi = \dfrac{C^* - C_\infty^*}{C_w^* - C_\infty^*}, j = \dfrac{V_0^2}{\nu^2} j^*, \gamma = j^*\left(\mu + \dfrac{\Lambda}{2}\right) = \mu\, j^*\left(1 + \dfrac{\beta}{2}\right), \beta = \dfrac{\Lambda}{2}, M = \sigma B_0^2\, \nu / \rho V_0^2, \\ K = V_o^2\, K^*/\nu^2,\ Sc = \nu / D_m, \Pr = \nu\,\rho\, Cp/\kappa = \mu Cp/\kappa, Gr = \nu\beta_T g^*\left(T_w^* - T_\infty^*\right)/U_0 V_0^2, \\ Gm = \nu\beta_C g^*\left(C_w^* - C_\infty^*\right)/U_0 V_0^2, R = 16\bar{\sigma}\, T_\infty^3 / 3k\,\bar{k}, Q = Q^*\nu^2 / V_0^2 k, \\ E_c = V_0^2 / C_p\left(T_w^* - T_\infty^*\right), Kr = Kr^*\nu / V_0^2 \end{array} \tag{11}$$

Using Eqs. (6)-(11) in (2)-(5) and dropping stars the governing equations and the boundary conditions in the non-dimensional form are:

$$\frac{\partial u}{\partial t} - \frac{\partial u}{\partial \eta} = (1+\beta)\frac{\partial^2 u}{\partial \eta^2} + (Gr\ \theta + Gm\ \phi) - N\ u + 2\beta\frac{\partial \omega}{\partial \eta} \tag{12}$$

$$\frac{\partial \omega}{\partial t}-\frac{\partial \omega}{\partial \eta}=\frac{1}{\lambda}\frac{\partial^2 \omega}{\partial \eta^2} \tag{13}$$

$$\frac{\partial \theta}{\partial t}-\frac{\partial \theta}{\partial \eta}=\frac{1}{\Gamma}\frac{\partial^2 \theta}{\partial \eta^2}-\frac{Q}{\Pr}\theta+Ec(1+\beta)\left(\left(\frac{\partial u}{\partial \eta}\right)^2+Mu^2\right) \tag{14}$$

$$\frac{\partial \phi}{\partial t}-\frac{\partial \phi}{\partial \eta}=\frac{1}{Sc}\frac{\partial^2 \phi}{\partial \eta^2}-Kr\,\phi \tag{15}$$

Dimensionless initial and boundary conditions are

$$\lambda=\mu\, j^*/\gamma=2/2+\beta, \tag{16}$$

where $\lambda=\mu\, j^*/\gamma_0=2/2+\beta,$ dimensionless gyro-viscosity, material parameter $\Gamma=\left(1-\frac{4}{3R+4}\right)Pr,$ and $N=\left(M+\frac{1}{K}\right).$

The physical quantities of interest used in materials processing simulations and design are Skin friction coefficient at the porous plate is written as

$C_f=\frac{2\,\tau_w^*}{\rho U_O V_O},$ where

$$\tau_w^*=(\mu+\Lambda)\frac{\partial u^*}{\partial y^*}\bigg|_{y^*=0}+\Lambda\,\omega^*\big|_{y^*=0} \tag{17}$$

The couple stress coefficient at the porous plate is written as

$C_m=\frac{M_w}{\mu\, j U_O},$ where

$$M_w=(\gamma)\frac{\partial \omega^*}{\partial y^*}\bigg|_{y^*=0} \tag{18}$$

Heat transfer coefficient and mass transfer coefficient at the porous plate in terms of Nusselt number and Sherwood number, as follows

$$Nu_x=x\frac{\left(\frac{\partial T}{\partial y^*}\right)_{y^*=0}}{\left(T_w^*-T_\infty^*\right)},\quad \text{and}$$

$$Sh_x=-x\frac{\left(\frac{\partial C}{\partial y^*}\right)_{y^*=0}}{\left(C_w^*-C_\infty^*\right)} \tag{19}$$

Converting (17)-(19) in the non-dimensional form are obtained as follows

Skin-friction is obtained as,

$$C_f = (1+\beta)\left(\frac{\partial u}{\partial \eta}\right)_{\eta=0} \tag{20}$$

Wall couple stress is defined as,

$$C_w = -\left(1+\frac{\beta}{2}\right)\left(\frac{\partial \omega}{\partial \eta}\right)_{\eta=0} \tag{21}$$

The non-dimensional form of Nusselt number is computed as

$$Nu / \mathrm{Re}_x = -(1+R)\left[\frac{\partial \theta}{\partial \eta}\right]_{\eta=0} \tag{22}$$

The non-dimensional form of Sherwood number is evaluated as

$$Sh / Re_x = -\left[\frac{\partial \phi}{\partial \eta}\right]_{\eta=0} \tag{23}$$

where $Re_x = \frac{V_o x}{\nu}$, local Reynolds number.

3 Numerical solution

The set of unsteady, reduced, non-dimensional, coupled partial differential Eqs. (12)-(15) under initial and boundary conditions (16) are non-linear and coupled, and therefore cannot be solved analytically. The finite element method (FEM) is the most popular and adoptable method for solving ordinary as well as partial differential equations. It is equally versatile at solving Newtonian and non-Newtonian problems. The details of the *variational* fi nite element method are documented succinctly in Reddy et al. [Reddy (1985); Rao (1989); Beg, Rashidi and Bhargava (2011)]. The fundamental steps in finite-element analysis are 1) Finite element discretization 2) Derivation of element equations 3) Assembly of element equations 4) Imposition of boundary conditions 5) Solution of assembled equations, which are briefly described in Shamshuddin et al. [Shamshuddin, Beg, Ram et al. (2017)] and the resulting final matrix equation obtained can be solved by any efficient iterative scheme.

3.1 Variational formulation

The variational formulation associated with Eqs. (12)-(15) over a typical two-node linear element $(\eta_e,\ \eta_{e+1})$ is given by:

$$\int_{\eta_e}^{\eta_{e+1}} w_1\left[\frac{\partial u}{\partial t} - \left(\frac{\partial u}{\partial \eta}\right) - A_1\left(\frac{\partial^2 u}{\partial \eta^2}\right) - (Gr\theta + Gc\phi) + N(u) - A_2\left(\frac{\partial \omega}{\partial \eta}\right)\right] d\eta = 0 \tag{24}$$

$$\int_{\eta_e}^{\eta_{e+1}} w_2\left[\frac{\partial \omega}{\partial t} - \left(\frac{\partial \omega}{\partial \eta}\right) - A_3\left(\frac{\partial^2 \omega}{\partial \eta^2}\right)\right] d\eta = 0 \tag{25}$$

$$\int_{\eta_e}^{\eta_{e+1}} w_3 \left[\frac{\partial \theta}{\partial t} - \left(\frac{\partial \theta}{\partial \eta} \right) - A_4 \left(\frac{\partial^2 \theta}{\partial \eta^2} \right) + \frac{Q}{\Pr} \theta - A_1 Ec \left(\left(\frac{\partial u}{\partial \eta} \right)^2 + Mu^2 \right) \right] d\eta = 0 \tag{26}$$

$$\int_{\eta_e}^{\eta_{e+1}} w_4 \left[\frac{\partial \phi}{\partial t} - \left(\frac{\partial \phi}{\partial \eta} \right) - \frac{1}{Sc} \left(\frac{\partial^2 \phi}{\partial \eta^2} \right) + Kr\, \phi \right] d\eta = 0 \tag{27}$$

where $A_1 = 1 + \beta$, $A_2 = (2\beta)$, $A_3 = \frac{1}{\tau}$ $A_4 = \frac{1}{\Gamma}$ and w_1, w_2, w_3, w_4 are arbitrary test functions and may be viewed as the variations in u, ω, θ and ϕ respectively. After dropping the order of integration and non-linearity, we arrive at the following system of equations

$$\int_{\eta_e}^{\eta_{e+1}} \left[(w_1) \frac{\partial u}{\partial t} - (w_1) \frac{\partial u}{\partial \eta} + A_1 \frac{\partial w_1}{\partial \eta} \frac{\partial u}{\partial \eta} + N(w_1) u - \left[Gr(w_1) \theta + Gc(w_1) \phi \right] - A_2 (w_1) \frac{\partial \omega}{\partial \eta} \right] d\eta - \left[w_1 \left(\frac{\partial u}{\partial \eta} \right) \right]_{\eta_e}^{\eta_{e+1}} = 0 \tag{28}$$

$$\int_{\eta_e}^{\eta_{e+1}} \left[(w_2) \frac{\partial \omega}{\partial t} - (w_2) \frac{\partial \omega}{\partial \eta} + A_3 \left(\frac{\partial w_2}{\partial \eta} \right) \left(\frac{\partial \omega}{\partial \eta} \right) \right] d\eta - \left[(w_2) \left(\frac{\partial \omega}{\partial \eta} \right) \right]_{\eta_e}^{\eta_{e+1}} = 0 \tag{29}$$

$$\int_{\eta_e}^{\eta_{e+1}} \left[(w_3) \frac{\partial \theta}{\partial t} - (w_3) \frac{\partial \theta}{\partial \eta} + A_3 \left(\frac{\partial w_3}{\partial \eta} \right) \left(\frac{\partial \theta}{\partial \eta} \right) + \frac{Q}{\Pr} (w_3) \theta - A_1 Ec (w_3) \left(\left(\frac{\partial \bar{u}}{\partial y} \right) \left(\frac{\partial u}{\partial y} \right) + Mu^2 \right) \right] d\eta - \left[A_3 (w_3) \left(\frac{\partial \theta}{\partial \eta} \right) \right]_{\eta_e}^{\eta_{e+1}} = 0 \tag{30}$$

$$\int_{\eta_e}^{\eta_{e+1}} \left[(w_4) \frac{\partial \phi}{\partial t} - (w_4) \left(\frac{\partial \phi}{\partial \eta} \right) + \frac{1}{Sc} \left(\frac{\partial w_4}{\partial \eta} \right) \left(\frac{\partial \phi}{\partial \eta} \right) + Kr\, (w_4)\, \phi \right] d\eta - \left[\frac{(w_4)}{Sc} \left(\frac{\partial \phi}{\partial \eta} \right) \right]_{\eta_e}^{\eta_{e+1}} = 0 \tag{31}$$

3.2 Finite element formulation

The finite element model may be obtained from Eqs. (28)-(31) by substituting *finite element approximations* of the form:

$$\left.\begin{aligned} u &= \sum_{j=1}^{2} u_j^e \psi_j^e, \\ \omega &= \sum_{j=1}^{2} \omega_j^e \psi_j^e, \\ \theta &= \sum_{j=1}^{2} \theta_j^e \psi_j^e \\ &and \\ \phi &= \sum_{j=1}^{2} \phi_j^e \psi_j^e \end{aligned}\right\} \tag{32}$$

With $w_1 = w_2 = w_3 = w_4 = \psi_j^e \ (i = 1, 2)$, where u_j^e, ω_j^e, θ_j^e *and* ϕ_j^e are the velocity in the direction of *x*,*y*-axis and temperature respectively at the j^{th} node of typical e^{th} element (η_e, η_{e+1}) and ψ_i^e are the shape functions for this element (η_e, η_{e+1}) and are taken as:

$$\left.\begin{aligned} \psi_1^e &= \frac{\eta_{e+1} - \eta}{\eta_{e+1} - \eta_e} \\ &and \\ \psi_2^e &= \frac{\eta - \eta_e}{\eta_{e+1} - \eta_e}, \ \eta_e \le \eta \le \eta_{e+1} \end{aligned}\right\} \tag{33}$$

Hence e^{th} element thus formed is

$$\begin{bmatrix} [K^{11}] & [K^{12}] & [K^{13}] & [K^{14}] \\ [K^{21}] & [K^{22}] & [K^{23}] & [K^{24}] \\ [K^{31}] & [K^{32}] & [K^{33}] & [K^{34}] \\ [K^{41}] & [K^{42}] & [K^{43}] & [K^{44}] \end{bmatrix} \begin{bmatrix} \{U^e\} \\ \{\omega^e\} \\ \{\theta^e\} \\ \{\phi^e\} \end{bmatrix} + \begin{bmatrix} [M^{11}] & [M^{12}] & [M^{13}] & [M^{14}] \\ [M^{21}] & [M^{22}] & [M^{23}] & [M^{24}] \\ [M^{31}] & [M^{32}] & [M^{33}] & [M^{34}] \\ [M^{41}] & [M^{42}] & [M^{43}] & [M^{44}] \end{bmatrix} \begin{bmatrix} \{U'^e\} \\ \{\omega'^e\} \\ \{\theta'^e\} \\ \{\phi'^e\} \end{bmatrix} = \begin{bmatrix} \{b^{1e}\} \\ \{b^{2e}\} \\ \{b^{3e}\} \\ \{b^{4e}\} \end{bmatrix} \tag{34}$$

where $\{[K^{mn}], [M^{mn}]\}$ and $\{\{u^e\}, \{\omega^e\}, \{\theta^e\}, \{\phi^e\}, \{u'^e\}, \{\omega'^e\}, \{\theta'^e\}, \{\phi'^e\} and \{b^{me}\}\}$

(*m*,*n*=1,2,3,4) are the set of matrices of order 2×2 and 2×1. *prime* $(')$ indicates $\frac{d}{d\eta}$.

These matrices are defined as follows:

$$\begin{cases} K_{ij}^{11} = -\int_{\eta_e}^{\eta_{e+1}} \left[\left(\psi_i^e\right)\left(\frac{\partial \psi_j^e}{\partial \eta}\right)\right] dy + A_1 \int_{y_e}^{y_{e+1}} \left[\left(\frac{\partial \psi_i^e}{\partial \eta}\right)\left(\frac{\partial \psi_j^e}{\partial \eta}\right)\right] d\eta, \\ K_{ij}^{12} = N \int_{\eta_e}^{\eta_{e+1}} \left(\psi_i^e\right)\left(\psi_j^e\right) d\eta, \; K_{ij}^{13} = -A_2 \int_{\eta_e}^{\eta_{e+1}} \left[\left(\psi_i^e\right)\left(\frac{\partial \psi_j^e}{\partial \eta}\right)\right] d\eta, \\ K_{ij}^{14} = -\left[Gr + Gm\right] \int_{\eta_e}^{\eta_{e+1}} \left(\psi_i^e\right)\left(\psi_j^e\right) d\eta, \\ M_{ij}^{11} = \int_{\eta_e}^{\eta_{e+1}} \left(\psi_i^e\right)\left(\psi_j^e\right) d\eta, \quad M_{ij}^{12} = M_{ij}^{13} = M_{ij}^{14} = 0 \end{cases} \tag{35}$$

$$\begin{cases} K_{ij}^{21} = -\int_{\eta_e}^{\eta_{e+1}} \left[\left(\psi_i^e\right)\left(\frac{\partial \psi_j^e}{\partial \eta}\right)\right] d\eta, \; K_{ij}^{22} = -A_3 \int_{\eta_e}^{\eta_{e+1}} \left[\left(\frac{\partial \psi_i^e}{\partial \eta}\right)\left(\frac{\partial \psi_j^e}{\partial \eta}\right)\right] d\eta, \\ K_{ij}^{23} = 0, \; K_{ij}^{24} = 0 \\ M_{ij}^{21} = 0, \; M_{ij}^{22} = \int_{\eta_e}^{\eta_{e+1}} \left(\psi_i^e\right)\left(\psi_j^e\right) d\eta, \; M_{ij}^{23} = M_{ij}^{24} = 0, \end{cases} \tag{36}$$

$$\begin{cases} K_{ij}^{31} = -A_1 Ec \int_{\eta_e}^{\eta_{e+1}} \left(\psi_i^e\right)\left(\frac{\partial \bar{u}}{\partial \eta}\right)\left(\frac{\partial \psi_j^e}{\partial \eta}\right) d\eta - A_1 Ec\, M \int_{\eta_e}^{\eta_{e+1}} \left(\left(\psi_i^e\right)\left(\psi_j^e\right)\right)^2 d\eta, \\ K_{ij}^{32} = -\int_{\eta_e}^{\eta_{e+1}} \left[\left(\psi_i^e\right)\left(\frac{\partial \psi_j^e}{\partial \eta}\right)\right] d\eta + A_4 \int_{\eta_e}^{\eta_{e+1}} \left[\left(\frac{\partial \psi_i^e}{\partial \eta}\right)\left(\frac{\partial \psi_j^e}{\partial \eta}\right)\right] d\eta, \\ K_{ij}^{33} = \frac{Q}{\Pr} \int_{\eta_e}^{\eta_{e+1}} \left[\left(\psi_i^e\right)\left(\psi_j^e\right)\right] d\eta, \quad K_{ij}^{34} = 0, \\ M_{ij}^{31} = 0, \; M_{ij}^{32} = 0, M_{ij}^{33} = \int_{\eta_e}^{\eta_{e+1}} \left(\psi_i^e\right)\left(\psi_j^e\right) d\eta, \quad M_{ij}^{34} = 0 \end{cases} \tag{37}$$

$$\begin{cases} K_{ij}^{41}=0, \\ K_{ij}^{42}=-\int_{\eta_e}^{\eta_{e+1}}\left[\left(\psi_i^e\right)\left(\frac{\partial\psi_j^e}{\partial\eta}\right)\right]d\eta+\frac{1}{Sc}\int_{\eta_e}^{\eta_{e+1}}\left[\left(\frac{\partial\psi_i^e}{\partial\eta}\right)\left(\frac{\partial\psi_j^e}{\partial\eta}\right)\right]d\eta, \\ K_{ij}^{43}=K_r\int_{\eta_e}^{\eta_{e+1}}\left(\psi_i^e\right)\left(\psi_j^e\right)d\eta,\ K_{ij}^{44}=0, \\ M_{ij}^{41}=0,\ M_{ij}^{42}=0,\ M_{ij}^{43}=\int_{\eta_e}^{\eta_{e+1}}\left(\psi_i^e\right)\left(\psi_j^e\right)d\eta,\ M_{ij}^{44}=0 \end{cases} \tag{38}$$

$$\begin{cases} b_i^{1e}=\left[\left(\psi_i^e\right)\left(\frac{\partial u}{\partial\eta}\right)\right]_{\eta_e}^{\eta_{e+1}},\ b_i^{2e}=\left[\left(\psi_i^e\right)\left(\frac{\partial\omega}{\partial\eta}\right)\right]_{\eta_e}^{\eta_{e+1}}, \\ b_i^{3e}=\left[A_3\left(\frac{\partial\theta}{\partial\eta}\right)\right]_{\eta_e}^{\eta_{e+1}},\ b_i^{4e}=\left[\frac{\left(\psi_i^e\right)}{Sc}\left(\frac{\partial\phi}{\partial\eta}\right)\right]_{\eta_e}^{\eta_{e+1}} \end{cases} \tag{39}$$

In general, to verify that the converged solutions are indeed correct, i.e., to guarantee grid (mesh) independency, a *grid refinement test* is carried out by dividing the whole domain into successively sized grids 81×81, 101×101 and 121×121 in the *z*-axis direction. Furthermore, the finite element code is run for different grid sizes and for a grid size of 101×101 the solutions are observed to achieve mesh independence. Therefore, for all subsequent computations, a grid size of 101 intervals is elected, with a step size 0.01 and hence a set of 404*non-linear* equations are solved with an iterative scheme. Finally, the solution is assumed to be convergent when the iterative process is terminated when the following condition is fulfilled:

$$\sum_{i,j}\left|\xi^{n+1}-\xi^{n}\right|\le 10^{-6} \tag{40}$$

where $\xi=u,\omega,\theta,\phi$ and n denotes the iterative step. This criterion maintains high accuracy for coupled multi-physical boundary layer equations. Once the key variables are computed, many wall gradient functions may be automatically evaluated.

4 Validation of numerical results

To validate and accuracy of the numerical results obtained by adopting Galerkin finite element method, weighted residual approach in the present analysis, we have compared with the analytical result of earlier published [Roja, Reddy and Reddy (2013)] in the absence of heat absorption and chemical reaction parameter which is depicted in Tabs. 1 and 2 and these favorable comparisons lend high confidence in the present finite element code accuracy. Tabs. 3 and 4 depicts for the general model with all parameters invoked. From Tab. 3 clearly, it is noticed that as heat absorption parameter Q increases as C_f, C_w decreases and Nu increases.

Table 1: Effects of $\beta, M, Gr \text{ and } Gm$ on $C_f, C_w, Nu/\mathrm{Re}_x \text{ and } Sh/\mathrm{Re}_x$ when $Q = 0, Kr = 0$

				Previous results			
β	M	Gr	Gm	C_f	C_w	Nu/Re_x	Sh/Re_x
0.1	2.0	2.0	2.0	0.6444	0.6446	0.4269	0.6008
0.5	2.0	2.0	2.0	0.5991	0.5990	0.4274	0.6008
0.5	**1.0**	2.0	2.0	1.0339	1.0338	0.4263	0.6008
0.5	2.0	**4.0**	2.0	1.6116	1.6113	0.4240	0.6008
0.5	2.0	2.0	**1.0**	3.8376	3.8434	-12.4087	0.6008
				Present results (FEM)			
0.1	2.0	2.0	2.0	0.644403	0.644603	0.426902	0.600803
0.5	2.0	2.0	2.0	0.599107	0.599005	0.427404	0.600803
0.5	**1.0**	2.0	2.0	1.033911	1.033809	0.426301	0.600803
0.5	2.0	**4.0**	2.0	1.611661	1.611420	0.424001	0.600803
0.5	2.0	2.0	**1.0**	3.837605	3.843918	-12.408605	0.600803

Sh shows no variations. Furthermore, as Kr increases, C_f C_w both decreases. However, for higher values of Kr, a significant increase in Sherwood number Sh is observed.

Table 2: Effects of $Ec, R \text{ and } Sc$ on $C_f, C_w, Nu/\mathrm{Re}_x \text{ and } Sh/\mathrm{Re}_x$ when $Q = 0, Kr = 0$

			Previous results			
Ec	R	Sc	C_f	C_w	Nu/Re_x	Sh/Re_x
0.01	2.0	0.6	0.5991	0.5990	0.4253	0.6008
1.0	2.0	0.6	0.5076	0.5075	0.6011	0.6008
0.01	**1.0**	0.6	0.6740	0.6739	0.3046	0.6008
0.01	2.0	**0.8**	0.5125	0.5124	0.4265	0.8010
			Present results (FEM)			
0.01	2.0	0.6	0.599107	0.599005	0.425305	0.600803
1.0	2.0	0.6	0.507619	0.507521	0.601118	0.600803
0.01	**1.0**	0.6	0.674006	0.673910	0.304619	0.600803
0.01	2.0	**0.8**	0.512507	0.512411	0.426506	0.801001

Table 3: Effects of various parameters on $C_f, C_w, Nu/\mathrm{Re}_x \text{ and } Sh/\mathrm{Re}_x$ for Kr with $t = 1, n = 0.1, \varepsilon = 0.01, Up = 0.5, \beta = 0.5, M = 2, Gr = 2, Gm = 2, \mathrm{Pr} = 0.71, R = 2, Ec = 0.01, Kr = 0.5$

Parameter	values	C_f	C_w	Nu/Re_x	Sh/Re_x
	0.5	2.7196	2.7447	0.5785	1.1762
Q	1.0	2.7073	2.7338	0.5785	1.4786

Table 4: Effects of various parameters on C_f, C_w, Nu/Re_x *and* Sh/Re_x for Kr with $t=1, n=0.1, \varepsilon=0.01, Up=0.5, \beta=0.5, M=2, Gr=2, Gm=2, \mathrm{Pr}=0.71, R=2, Q=0.5, Ec=0.01$

Parameter	values	C_f	C_w	Nu/Re_x	Sh/Re_x
	1.0	2.4215	2.7313	0.5663	1.4615
Kr	2.0	2.3312	2.7215	0.5663	1.4821

5 Results and discussion

Unsteady flow of micropolar electrically conducting fluid over a vertical plate through porous has been investigated in the present study. The computations of velocity, Angular velocity, temperature, and concentration profiles are plotted through Figs. 2-19 and discussed the physical significance of thermo-physical parameters. Throughout the computation procedure, we have taken $t=1,\ n=0.1$. The permeability in all the figures plotted is set at 0.5 which corresponds to a highly porous regime. The value of $\mathrm{Pr}=0.71$ (air) and $Sc=0.6$ (water-vapor).

The heat absorption parameter Q appearing in (14) is the dimensionless parameter based on term $Q^*\left(T^*-T_\infty^*\right)$, Q^* being constant coefficient. The source term represents heat absorption $Q<0$ and heat generation when $Q>0$. Fig. 2 depicts the effect of temperature on heat absorption parameter Q. Existence of the heat absorption effect has the tendency to repress the fluid temperature. These behaviors are obvious from Fig. 2 that temperature distributions decrease as Q increases.

Fig. 3 exhibits the effects of the Eckert number Ec on the temperature profiles. Eckert number characterizes the heat dissipation which is advective transport with respect to heat dissipation potential. It is observed that an increasing Ec the temperature of the fluid increases in the thermal boundary layer. However, higher values of Eckert number, temperature decreases significantly (Fig. 3). It is since internal energy is increased in the free stream indicates that an adequately large infinity boundary condition has been imposed in the finite element model.

The profiles of the temperature in the boundary layer for various values of Prandtl number Pr are shown in Fig. 4. Prandtl number represents the relative rate of momentum diffusion to energy diffusion. For $\mathrm{Pr}<1$ energy, diffusion rate exceeds momentum diffusion. Also, fluids with higher Prandtl number possess greater viscosities and as Pr increases from 0.71 through 1 to 5. Temperature is significantly suppressed with greater Prandtl number, as plotted in Fig. 4, Greater Prandtl number corresponds to lower thermal conductivity. This leads to a reduction in thermal energy convected through the fluid from the plate. A similar trend can be observed in many articles related to micropolar including Roja et al. [Roja, Reddy and Reddy (2013)].

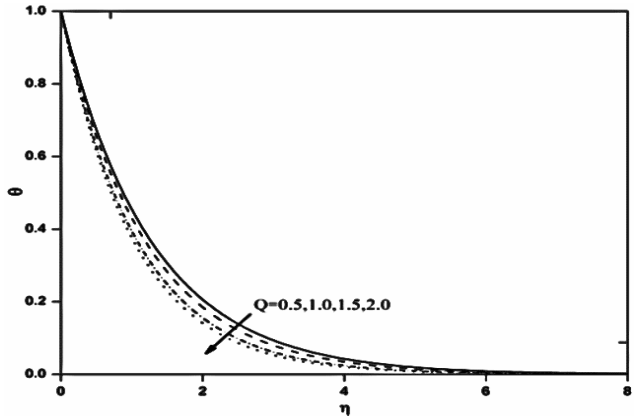

Figure 2: Effect of heat absorption Q on velocity u

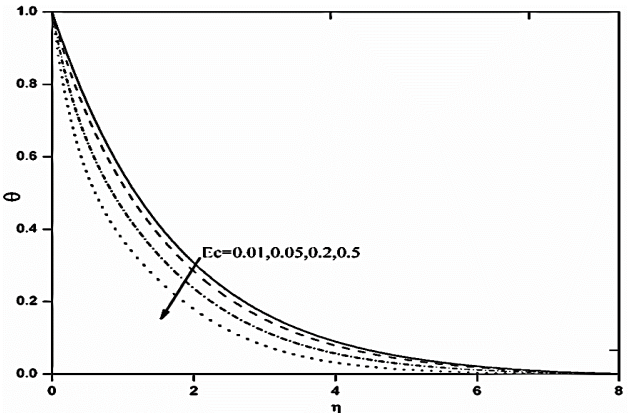

Figure 3: Effect of Eckert number Ec on velocity u

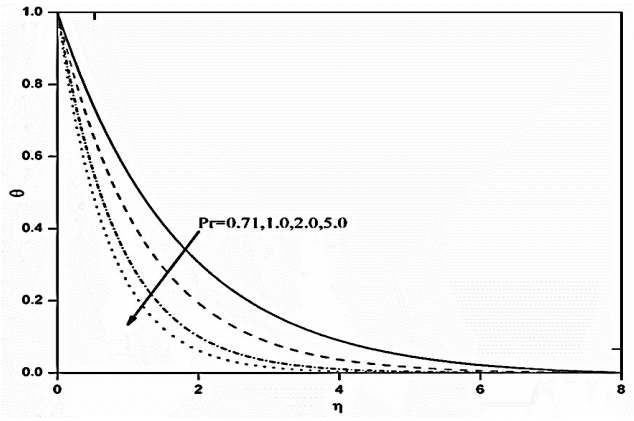

Figure 4: Effect of Prandtl number Pr on velocity u

Fig. 5 presents the effect of thermal radiation parameter R on temperature profiles. From the definition, $R = 16\bar{\sigma} T_{\infty}^{3} / 3k\,\bar{k}$, which appeared in the thermal diffusion term in Eq. (14) i.e., $(1/\Gamma)\left(\partial^2\theta/\partial\eta^2\right)$. R<1 represents the thermal radiation is dominated by thermal conduction. R=1 represents the contribution of both the thermal properties are equal and R>1 shows thermal radiation dominates over thermal conduction. In present simulations, we confine our discussion considering all these three cases. It is noticed from the present study that as R increases temperature profiles are markedly decreases.

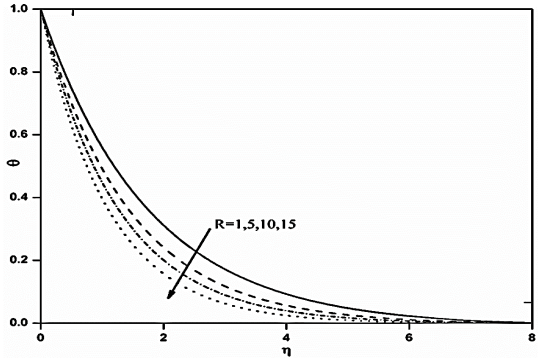

Figure 5: Effect of Radiation Parameter R on velocity u

The pattern of concentration profiles for chemical reaction parameter Kr and Schmidt number $Sc$are presented in Figs. 6-7. The present study, the destructive type of homogenous chemical reaction is considered. It is interesting to note that a sharp fall in concentration profile is marked with an increase in a chemical reaction. It is due to the fact that, when the chemical reaction takes place, a destructive chemical reaction destroys the original species. The term $Sc = \nu / D$ defines as the ratio of the momentum to the mass diffusivity. From the profiles, it is observed that the depression in concentration magnitudes is due to the reduction in molecular diffusivity which manifests in a stifled migration of species. Hence concentration profiles decrease as Sc increases.

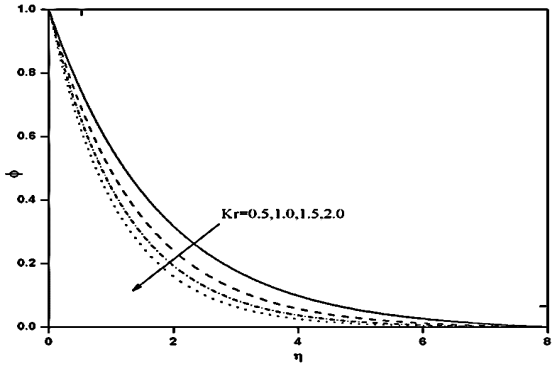

Figure 6: Effect of chemical reaction parameter Kr on concentration ↗

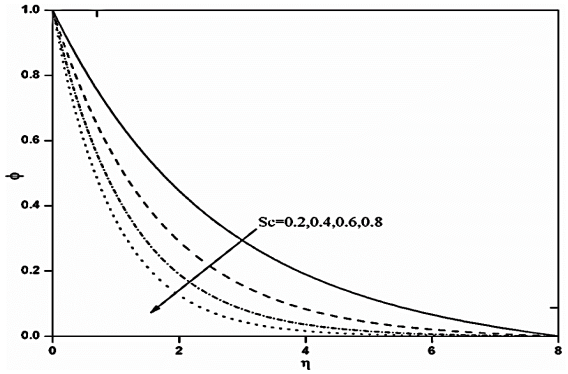

Figure 7: Effect of Schmidt number *Sc* on concentration ↗

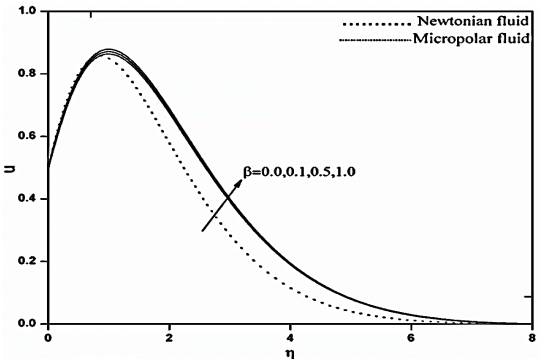

Figure 8: Effect of Eringen micropolar vortex viscosity parameter β on velocity u

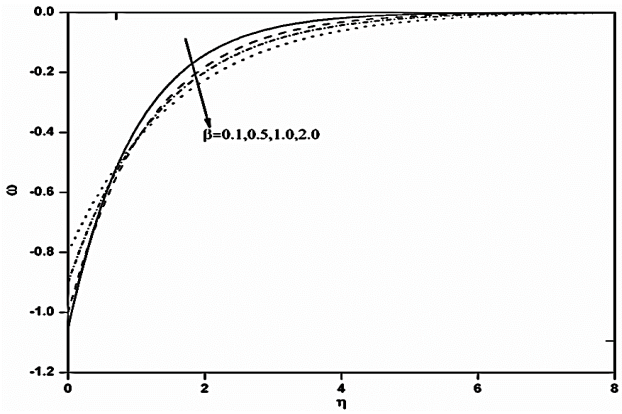

Figure 9: Effect of Eringen micropolar vortex viscosity parameter β on Microrotation ω

Figs. 8-9 illustrate the influence of β, the micro-rotation parameter on velocity and micro-rotation profiles respectively**.** It is evident that velocity distribution is greater for a Newtonian fluid (β=0) with the given parameters, as compared with non-Newtonian fluid (micropolar fluid). As β increases the peak values are attained close to the plate and

these migrate away from the plate, hence all profiles decay from the peak and disappear in the free stream velocity. In addition, the micro-rotation (Fig. 9) i.e., angular velocity takes negative values throughout the regime. Hence micro-rotation velocity profiles increase as β increases.

The response of Grashof number Gr and modified Grashof number Gm on velocity and microrotation profiles are depicted in Figs. 10-13. It is to note that, as Gr or Gm increases velocity profiles also increase. However, the reverse effect is encountered in case of micro-rotation profiles i.e., the profile decreases with an increasing value of both the buoyancy parameters. The said observation is due to the fact that Gr ,the relative measure of the magnitude of the thermal buoyancy and to that of the opposing frictional forces acting on the micropolar fluid and Gm , the relative measure of species buoyancy force to viscous hydrodynamic force.

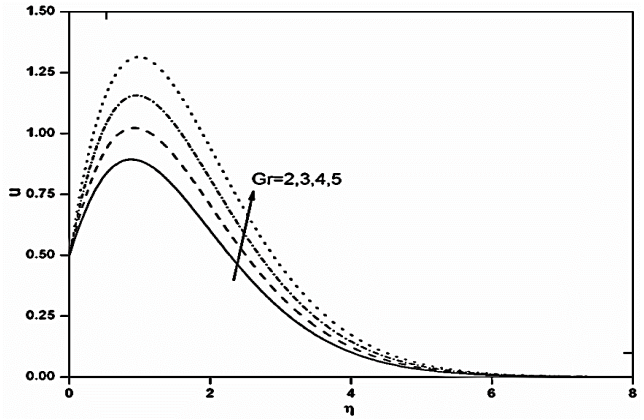

Figure 10: Effect of Thermal Grashof number Gr on velocity u

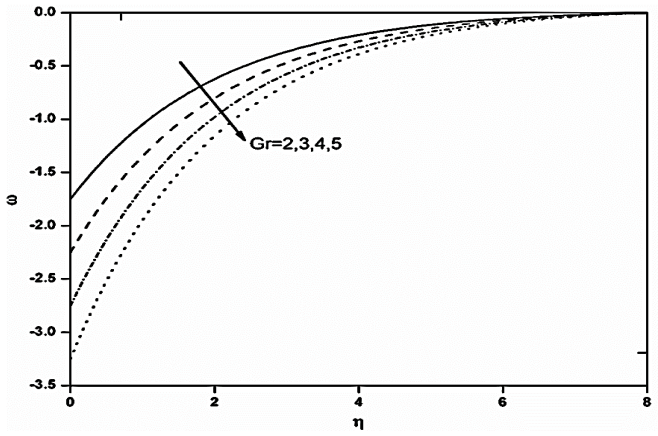

Figure 11: Effect of Thermal Grashof number Gr on Microrotation ω

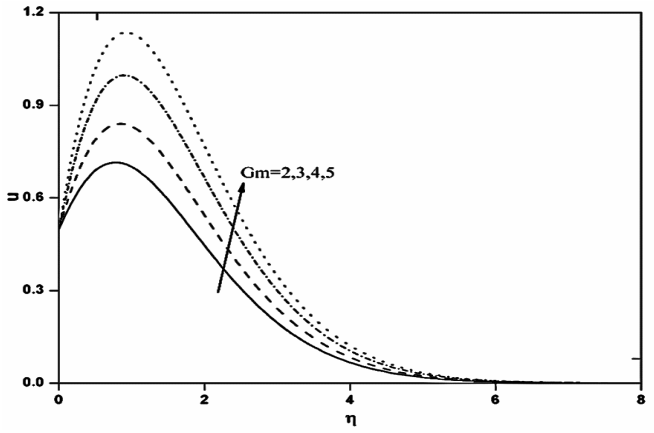

Figure 12: Effect of Solutal Grashof number Gm on velocity u

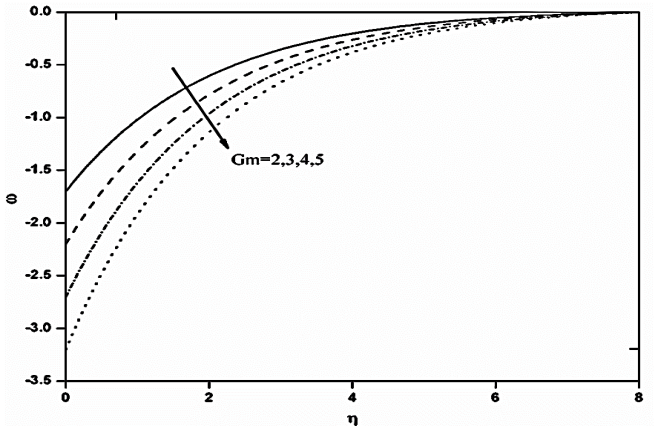

Figure 13: Effect of Solutal Grashof number Gm on Microrotation ω

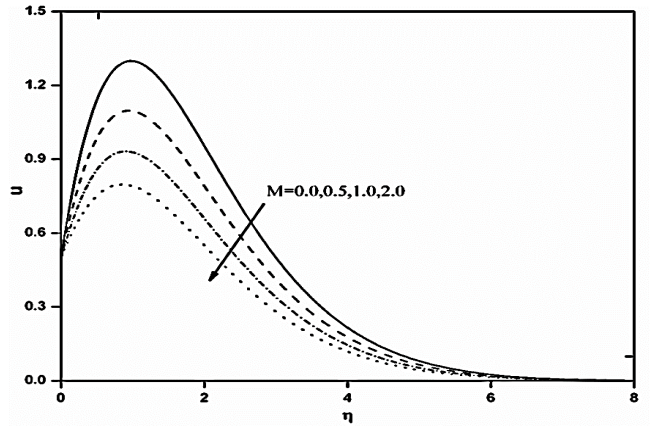

Figure 14: Effect of Magnetic field parameter M on velocity u

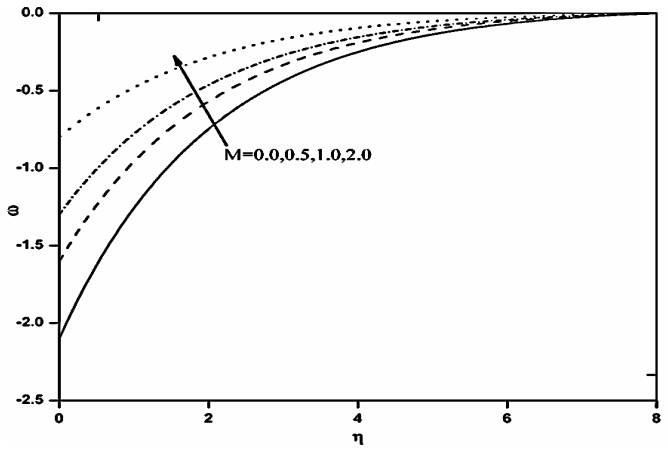

Figure 15: Effect of Magnetic field parameter M on Microrotation ω

Figs. 14-15 shows the variations in the velocity and angular velocity for various values of dimensionless magnetic field parameter M. Physically, in magneto-hydrodynamic material processing, the applied magnetic field caused by Lorentz force, is a resistive force which retards the velocity profile significantly. As a result, the boundary layer thickness also decreases. In the case of Fig. 15, the angular velocity profile enhances significantly with an increase in the magnetic parameter.

The pattern of velocity and microrotation profiles for permeability K are shown in Figs. 16-17. It is originated from drag force (Darcian) term in the composite linear momentum Eqn. (12), viz $-(1/K)u$ in a combined term N as mentioned in Eq. (12). As permeability quickly increases velocity near the wall of the porous plate increases. A similar trend is also found in case of microrotation i.e., as permeability increases microrotation velocity also increases.

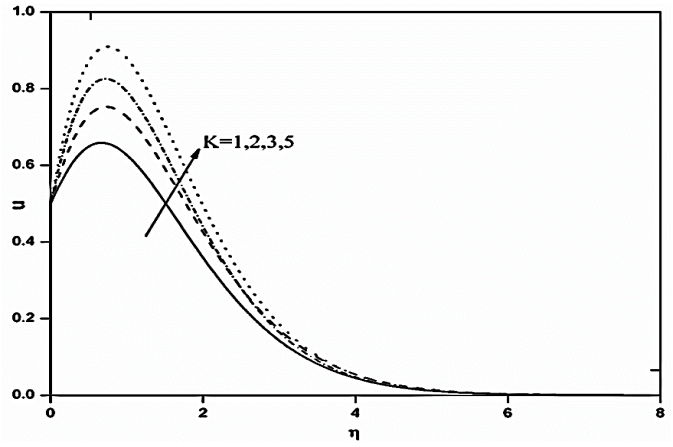

Figure 16: Effect of Permeability Parameter K on velocity u

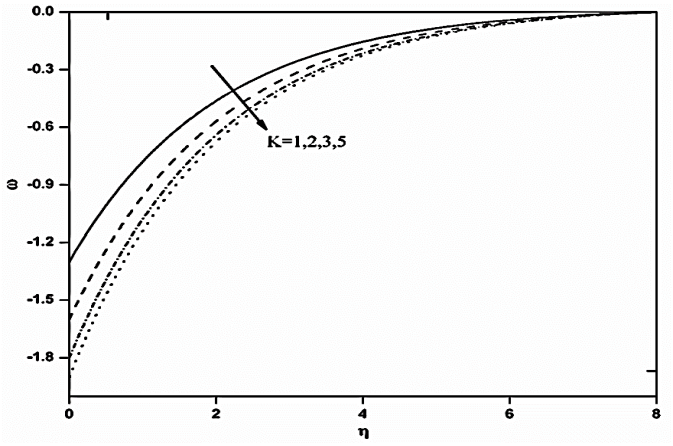

Figure 17: Effect of Permeability Parameter K on Microrotation ω

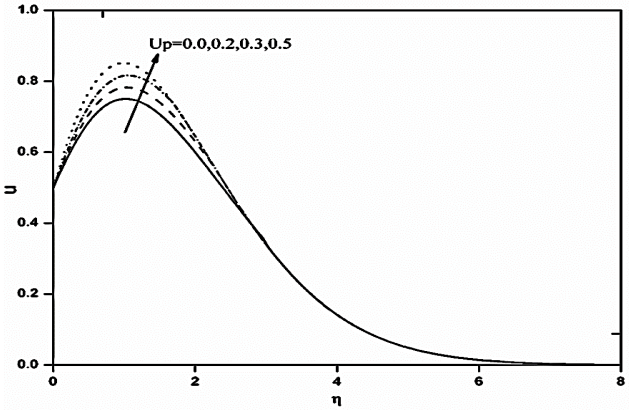

Figure 18: Effect of Plate Velocity U_P on velocity u

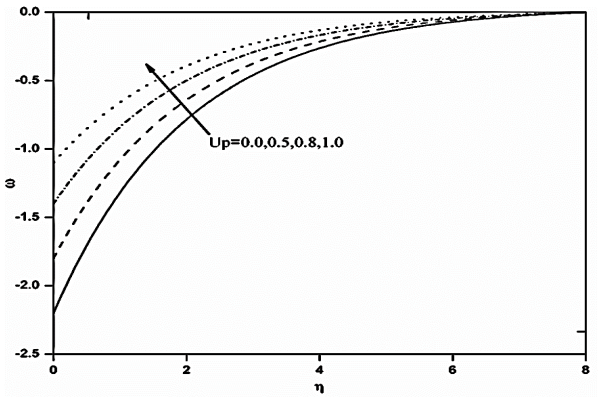

Figure 19: Effect of Plate Velocity U_P on Microrotation ω

Figs. 18-19 presents the graphical representation of dimensionless velocity and angular velocity profiles for some representative values of plate velocity. It is to be noted that the peak value of velocity across the boundary layer increases near the porous plate, also we observe the magnitude of microrotation on porous plate increases as U_p increases. Therefore, higher the plate velocity accelerates the linear flow whereas the micro-rotation decelerates.

6 Concluding remarks

In this work, a mathematical model for an unsteady, incompressible, electrically conducting micropolar fluid past a vertical plate in a porous media has been presented. Heat absorption in energy equation and chemical reaction effect in the solutal transfer equation have been included in the formulation. The conservation for momentum, angular momentum, energy, and concentration have been non-dimensionalized with appropriate variables. Based on the obtained solutions with the numerical scheme and using some graphical illustrations generated with the MATLAB software, for validation of present solutions, results are compared with the earlier published analytical solution of Roja et al. [Roja, Reddy and Reddy (2013)] and excellent correlation achieved. The main findings were the linear flow is accelerated and, in a consequence, the thickness of momentum boundary layer decreases with increasing values of microrotation parameter, plate velocity, thermal Grashof number, solutal Grashof number, and permeability parameter. A reverse phenomenon is observed in the case of the magnetic field parameter. Angular velocity (micro-rotation) is suppressed and micro-rotation boundary layer thickness increased with increasing of microrotation parameter, thermal Grashof number, solutal Grashof number, and permeability parameter. Conversely, angular velocity is elevated as plate velocity and magnetic field increases. Increasing Prandtl number, radiation-conduction parameter, heat absorption parameter, and Eckert number decrease temperature profiles. Increasing Schmidt number, first-order chemical reaction parameter decreases concentration values and reduces concentration boundary layer thickness. Sherwood number (wall mass transfer rate) is enhanced with increasing homogeneous chemical reaction, no variations in case of heat absorption parameter. Nusselt number (wall heat transfer rate) is enhanced with increasing heat absorption parameter, no variations in case of chemical reaction parameter.

The current simulations have shown the strong potential of finite element methods (FEM) in simulating realistic transport phenomena in heat exchange rheo-materials processing. Further studies will investigate alternate non-Newtonian models Eg. nanofluid particles in one-dimensional two-phase model with n-order chemical reaction will be communicated imminently.

References

Adunson, T.; Gebhart, B. (1972): An experimental and analytical study of natural convection with appreciable thermal radiation effects. *Journal of Fluid Mechanics*, vol. 52, pp. 57-95.

Alam, S.; Islam, T.; Uddin, M. J. (2016): Mathematical modelling for heat transfer of a micropolar fluid along a permeable stretching/shrinking wedge with heat

generation/absorption. *Mathematical Modelling of Engineering Problems*, vol. 3, no. 1, pp. 1-9.

Ariman, T.; Turk, M. A.; Sylvester, N. D. (1973): Applications of micro continuum fluid mechanics-a review. *International Journal of Engineering Science*, vol. 11, pp. 905-930.

Ariman, T.; Turk, M. A.; Sylvester, N. D. (1974): Applications of micro continuum fluid mechanics-a review. *International Journal of Engineering Science*, vol. 12, pp. 273-293.

Babu, M. S.; Kumar, S. G.; Reddy, T. S. (2013): Mass transfer effects on unsteady MHD convective flow of a micropolar fluid past a vertical moving porous plate through porous medium with viscous dissipation. *International Journal of Applied Mathematics and Mechanics*, vol. 9, no. 6, pp. 48-67.

Babu, M. S.; Lavanya, M.; Ramanaiah, G. V. (2015): Effect of heat generation/absorption on heat and mass transfer in a micropolar fluid over a stretching sheet with Newtonian heating and chemical reaction. *International Journal of Mathematics Trends and Technology*, vol. 28, no. 1, pp. 19-27.

Bala Rama Krishna, C.; Rama Chandra Rao, P. S.; Srikanth, D. (2014): Special multi-step method for a class of nonlinear boundary value problem. *International Journal of Mathematical Sciences and Engineering Applications*, vol. 8, no. 3, pp. 237-249.

Bég. O. A.; Rashidi, M. M.; Bhargava, R. (2011): *Numerical Simulation in Micropolar Fluid Dynamics*. Lambert: Sarbrucken. Germany.

Chen, C. H. (2004): Heat and mass transfer in MHD flow by natural convection from a permeable inclined surface with variable wall temperature and concentration. *Acta Meccanica*, vol. 172, pp. 219-235.

Cowin, S. C. (1968): Polar fluids. *Physics of Fluids*, vol. 11, pp. 1919-1927.

Cowling, T. G. (1957): *Magnetohydrodynamics*. New York: Wiley Inter Science.

Damesh, R. A.; Odat, M. Q.; Chamkha, A. J.; Shannk, A. B. (2009): Combined effect of heat generation/absorption and first-order chemical reaction on micropolar fluid flows over a uniform stretched permeable surface. *International Journal of Thermal Sciences*, vol. 48, pp. 1658-1663.

Eringen, A. C. (1966): A unified theory of thermomechanical materials. *International Journal of Engineering Science*, vol. 4, no. 2, pp. 179-202.

Eringen, A. C. (1966): Theory of micropolar fluids. *Journal of Applied Mathematics and Mechanics*, vol. 16, pp. 1-18.

Gebhart, B. (1962): Effect of viscous dissipation in natural convection. *Journal of Fluid Mechanics*, vol. 14, pp. 225-232.

Krishna, C.; Rao, P. (2014): Study of stability analysis for a class of fourth-order boundary value problems. *Applied Mathematics*, vol. 5, pp. 1887-1893.

Lukaszewicz, G. (1999): *Micropolar Fluids Modelling and Simulation*. Boston: Birkhauser Boston.

Modather, M.; Rashad, A. M.; Chamkha, A. J. (2009): An analytical study of MHD heat and mass transfer oscillatory flow of a micropolar fluid over a vertical permeable

plate in a porous medium. *Turkish Journal of Engineering and Environmental Sciences*, vol. 33, no. 4, pp. 245-257.

Pal, D.; Biswas, S. (2016): Perturbation analysis of magnetohydrodynamics oscillatory flow on convective-radiative heat and mass transfer of micropolar fluid in a porous medium with chemical reaction. *Engineering Science and Technology: An International Journal*, vol. 19, pp. 444-462.

Pal, D.; Talukdar, B. (2012): Perturbation technique for unsteady MHD mixed convection periodic flow, heat and mass transfer in micropolar fluid with chemical reaction in the presence of thermal radiation. *Central European Journal of Physics*, vol. 10, pp. 1150-1167.

Rahman, M. M. (2009): Convective flows of micropolar fluids from radiative isothermal porous surfaces with viscous dissipation and Joule heating. *Communication in Nonlinear Science and Numerical Simulation*, vol. 14, pp. 3018-3030.

Rahman, M. M.; Sultana, Y. (2008): Radiative heat transfer flow of micropolar fluid with variable heat flux in a porous medium. *Nonlinear Analysis: Modelling and Control*, vol. 13, pp. 71-87.

Rao, S. R. (1989): *The Finite Element Method in Engineering*, 2nd Edition. USA: BPCC Wheaton's Ltd. Exeter.

Rapits, A.; Perdikis, C. (1998): Viscoelastic flow by the presence of radiation. *ZAMP*, vol. 78, pp. 277-279.

Reddy, J. N. (1985): *An Introduction to the Finite Element Method*. McGraw-Hill Newyork.

Roja, P.; Reddy, T. S.; Reddy, B. N. (2013): Radiation and mass transfer effects on MHD free convective flow of a micropolar fluid past an infinite vertical porous moving plate embedded in a porous medium with viscous dissipation. *International Journal of Scientific and Research Publications*, vol. 3, no. 6, pp. 1-12.

Rout, P. K.; Sahoo, S. N.; Dash, G. C.; Mishra, S. R. (2016): Chemical reaction effect on MHD free convection flow in a micropolar fluid. *Alexandria Engineering Journal*, vol. 55, no. 3, pp. 2967-2973.

Shamshuddin, M. D.; Bég, O. A.; Ram, M. S.; Kadir, A. (2017): Finite element computation of multi-physical micropolar transport phenomena from an inclined moving plate in porous media. *Indian. Journal of Physics*, vol. 92, no. 2, pp. 215-230.

Shamshuddin, M. D.; Thirupathi, T. (2017); Soret and Dufour effects on unsteady MHD free convective flow of micropolar fluid with oscillatory plate velocity considering viscous dissipation effects. *Jurnal Teknologi*, vol. 79, no. 4, pp. 123-136.

Sharma, R.; Bhargava, R.; Singh, I. V. (2010): Combined effect of magnetic field and heat absorption on an unsteady free convection and heat transfer flow in a micropolar fluid past a semi-infinite moving plate with viscous dissipation using element-free Galerkin method. *Applied Mathematics and Computation*, vol. 217, no. 1, pp. 308-321.

Singh, K.; Kumar, M. (2016): Effect of thermal radiation on mixed convection flow of a micropolar fluid from an unsteady stretching surface with viscous dissipation and heat generation/absorption. *International Journal of Chemical Engineering*, vol. 4, pp. 1-10.

Siva Reddy, S.; Shamshuddin, M. D. (2015): Heat and mass transfer on the MHD flow of a micropolar fluid in the presence of viscous dissipation and chemical reaction. *Procedia Engineering*, vol. 127, pp. 885-892.

Siva Reddy, S.; Shamshuddin, M. D. (2016): Diffusion-thermo and chemical reaction effects on an unsteady MHD free convection flow in a micropolar fluid. *Theoretical and Applied Mechanics*, vol. 43, pp. 117-131.

Siva Reddy, S.; Thirupathi, T. (2016a): Double diffusive magnetohydro-dynamic free convective flow of nanofluids past an inclined porous plate employing tiwari and das model: FEM. *Journal of Nanofluids*, vol. 5, no. 6, pp. 802-816.

Siva Reddy, S.; Thirupathi, T. (2016b): Heat and mass transfer effects on natural convection flow in the presence of volume fraction for copper-water nanofluid. *Journal of Nanofluids*, vol. 5, no. 2, pp. 220-230.

Siva Reddy, S.; Thirupathi, T. (2016c): Numerical study of heat transfer enhancement in MHD free convection flow over vertical plate utilizing nanofluids. *Ain Shams Engineering Journal*, vol. 9, no. 4, pp. 1169-1180.

Thirupathi, T.; Anwar Beg, O.; Kadir, A. (2017a): Numerical study of heat source/sink effects on dissipative magnetic nanofluid flow from a non-linear inclined stretching/shrinking sheet. *Journal of Molecular Liquids*, vol. 232, pp. 159-173.

Thirupathi, T.; Chamkha, A.; Siva Reddy, S. (2017b): MHD natural convective flow of nanofluids past stationary and moving inclined porous plate considering temperature and concentration gradients with suction. *International Journal of Numerical Methods for Heat and Fluid Flow*, vol. 27, no. 8, pp. 1765-1794.

Thirupathi, T.; Mishra, S. R. (2018): Effect of viscous dissipation and Joule heating on MHD Jeffery nanofluid flow with and without multi-slip boundary conditions. *Journal of Nanofluids*, vol. 7, no. 3, pp. 516-526.

Stokes, V. K. (1984): *Theories of Fluids with Microstructure*. New York: Springer.

Ziaul Haque, M. D.; Mahmud Alam, M. D.; Ferdows, M.; Postelnicu, A. (2012): Micropolar fluid behaviors on steady MHD free convection and mass transfer flow with constant heat and mass fluxes, Joule heating and viscous dissipation. *Journal of King Saud University-Engineering Science*, vol. 24, pp. 71-84.